LARGE-t ELASTIC SCATTERING AND DIFFRACTION DISSOCIATION AT THE CERN SPS COLLIDER

UA4 Collaboration

V. Innocente
Ecole Polytechnique, Palaiseau, France

ABSTRACT

Proton-antiproton elastic scattering was measured at the centre-of-mass energies of 546 and 630 GeV in the four-momentum transfer range $.45 \leq -t \leq 2.2$ GeV^2. The t-distribution shows an exponential decrease with a pronounced break at $-t \sim .9$ GeV^2 followed by a more gentle decrease. Diffraction dissociation $\bar{p}p \to \bar{p}X$ was also studied. The pseudorapidity distribution of charged particles, produced in the fragmentation of the system X, is shown to be in striking agreement with the prediction of the Dual Parton Model.

We report recent measurements of proton-antiproton elastic scattering and diffraction dissociation at a centre-of-mass energies of 546 and 630 GeV, performed at the CERN $S\bar{p}pS$ Collider by the UA4 Collaboration [1]. Comparisons with theoretical expectations will be made for both reactions.

1. ELASTIC SCATTERING

Elastic events were detected by high resolution wire chambers and scintillation counters hodoscopes, placed in special movable sections of the vacuum pipe ("Roman pots")[2]. Data were collected during several Collider runs at $\sqrt{s}$ = 546 and 630 GeV. At the lower energy the betatron function at the crossing point in the horizontal and vertical plane were β_h = 2 m, β_v = 1 m for the low-β mode and β_h = 1.3 m, β_v = 0.65 m for the squeezed-β mode. At $\sqrt{s}$ = 630 GeV the corresponding figures were β_h = 1 m and β_v = 0.5 m.

With these optics our detectors covered the angular range $2.5 \leq \Theta \leq 4.6$ mrad in the low-β mode and $2.8 \leq \Theta \leq 4.6$ mrad in the squeezed-β mode (the upper limits being due to the shape of the machine quadrupoles placed just in front of the inner pots). These figures correspond to a t-range of $.45 \leq -t \leq 1.55$ GeV^2 at $\sqrt{s}$ = 546 GeV that becomes $.7 \leq -t \leq 2.2$ GeV^2 at $\sqrt{s}$ = 630 GeV.

The trigger was provided by the left-right coincidence of the trigger counters of two opposite arms. It was a 6-fold coincidence for the low-β and a 8-fold coincidence for the squeezed-β mode. The deflection through the machine quadrupoles ensured that particles coming from the crossing region and accepted by the trigger had a momentum within about 10% of the beam momentum[14]. Calibration and detection efficiency of the wire chambers were studied using the data collected with the elastic trigger itself. In the track reconstruction procedure a hit was required in at least five of the eight drift planes and in at least one of two proportional planes in a telescope. Due to the redundancy in the number of planes a fully efficient detection could be ensured over the telescope acceptance.

The analysis was carried out according to the following steps:

(a) A single track was demanded in each telescope of two opposite arms without tracks in the other telescopes.

(b) Events were rejected if a hit was present in a system[2] of scintillation counter hodoscopes covering the pseudorapidity range $2.5 \leq |\eta| \leq 5.6$ on both sides of the crossing region.

(c) A three-standard-deviation cut was applied to the distributions of the vertical coordinate y_o of the proton and antiproton trajectories at the centre of the crossing region. A cut on the quantity y_o is equivalent to a momentum analysis on both scattered particles: a three-standard-deviation cut corresponds to a selection of events where the momentum of both p and $\bar{p}$ is within 2% of the beam momentum. The natural momentum spread of the circulating beam is only a few times 10^{-4}.

(d) A three-standard-deviation cut was then applied to the collinearity distributions of the proton and antiproton trajectories in the vertical plane.

The uncertainty on the scattering angle is determined by the intrinsic angular spread of the beam. The observed width of the collinearity distributions provides a direct measurement of this quantity which agrees well with the value calculated from the known machine parameters. The r.m.s. value of the t-resolution was $\Delta t = 0.06\sqrt{|t|}$ at $\sqrt{s}$ = 546 GeV and $\Delta t = 0.08\sqrt{|t|}$ at $\sqrt{s}$ = 630 GeV.

The position and the angle of the beam at the crossing point were continuously monitored during the data taking and checked comparing the trend of the observed angular distributions for the two arms (up-left x down-right) and (down-left x up-right).

The geometrical acceptance of the detectors as a function of t was carefully studied by varying the accepted interval of Θ_h (the horizontal component of the scattering angle) in order to ensure clearance inside the quadrupole vacuum chamber. The acceptance was calculated with a Monte-Carlo that takes into account the size, the angular spread and the angle of the incoming beams. It was checked that the t-dependence of the data remained the same when further reducing the accepted interval of $|\Theta_h|$.

The actual value of the scattering angle was calculated by taking the average of the observed production angles of the proton and antiproton, corrected for the beam angle.

The absolute normalization of the elastic differential cross sections at $\sqrt{s}$ = 546 GeV was obtained by smoothly joining the data points to previous measurements[3] at lower momentum transfer, which, in turn, were normalized to the optical point[4]. An alternative method is based on the use of a luminosity monitor which consists of the left-right coincidence of scintillation counters covering the angular range from .4° up to 1.5°, symmetrically on both sides of the crossing region. At $\sqrt{s}$ = 546 GeV the monitor detected 86% of the inelastic non diffractive cross section. No elastic scattering data at low-t being available at $\sqrt{s}$ = 630 GeV, we have normalized the elastic rates measured at this energy to the elastic cross section at $\sqrt{s}$ = 546 GeV using the ratio of the counting rates of the luminosity monitor as taken at the two energies. A 2% correction was applied to account for the energy dependence of the effective monitor cross section.

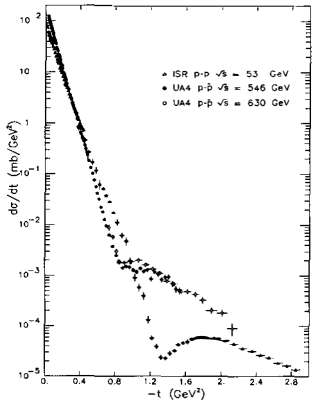

Fig. 1 Elastic scattering at the $\bar{p}pS$ Collider. Results at $\sqrt{s}$ = 546 and 630 GeV are compared with pp data at the ISR[7] ($\sqrt{s}$ = 53 GeV).

Results from the present experiment[5,6] are shown in fig. 1 compared with pp data measured at ISR at $\sqrt{s}$ = 53 GeV[7].

The data show an exponential decrease with momentum transfer up to $-t \sim .9$ GeV^2 followed by a shoulder with no sign of the dip, present in the ISR pp data. The cross section at the second maximum is more than one order of magnitude higher than at the ISR. In the momentum transfer region $1.1 \leq -t \leq 2.2$ GeV^2 covered at $\sqrt{s}$ = 630 GeV the data can be fitted using a simple exponential, $d\sigma/dt \sim \exp(bt)$, with a slope $b = 2.7 \pm 0.1$ GeV^{-2}. As can be seen in fig. 1, the differential cross section at $-t \simeq 2$ GeV^2 still remains larger than at the ISR. However, the trend of the Collider data is such that, as the momentum transfer increases, they seem to approach the ISR data.

Proton-antiproton elastic scattering in the energy region from the ISR to the SPS Collider, and beyond, has been recently discussed in several theoretical papers (ref. 10 for a recent review) where also definite predictions are made concerning the kinematic range covered in the present experiment.

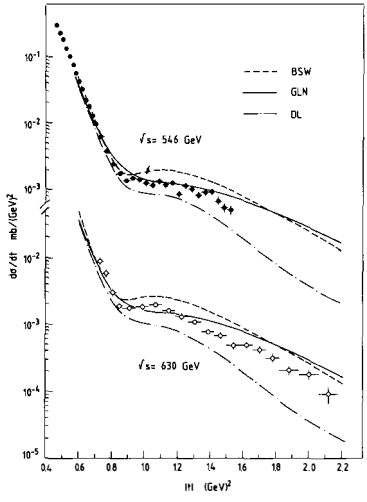

Fig. 2 UA4 results at $\sqrt{s}$ = 546 and 630 GeV in the break-shoulder region compared with theoretical predictions. Curves are from ref. 10.

In fig. 2 our data are compared with predictions from some current models of hadron elastic scattering. Two of these models from Donnachie and Landshoff DL[11] and from Gauron, Leader and Nicolescu GLN[12] account for the difference on shape between Collider and ISR data to the presence of an odd contribution to the elastic amplitude dominant at large-t. These models predict also a different shape in $\bar{p}p$ and pp scattering as observed at $\sqrt{s}$ = 53 GeV at the ISR[8,9]. In contrast with the two above quoted approaches, most of the existing models, based mainly on a geometrical picture of the hadron collision, as the one from Bourrely, Soffer and Wu BSW[13] also presented in fig. 2, predict that $\bar{p}p$ and pp elastic cross sections approach each other as the energy increase in conflict with the $\sqrt{s}$ = 53 GeV data.

2. DIFFRACTION DISSOCIATION

The reaction $\bar{p}p \to \bar{p}X$ was studied at the centre-of-mass energy $\sqrt{s} = 546$ GeV. The antiproton scattered at very small angles was observed in the elastic detectors discussed above. Charged particles produced by the proton fragmentation were observed in the vertex detector consisting of the UA4 counters and drift chamber telescopes, and of the central detector of the UA2 Collaboration. The trigger required a particle through the "Roman pot" telescopes on the outgoing antiproton side, in coincidence with at least one charged particle in the pseudorapidity range $2.5 \leq \eta \leq 5.6$ in the proton hemisphere. Events were analyzed by requiring the presence of an interaction vertex, reconstructed by the vertex detector, and of a single track in the "Roman pot" telescopes. The antiproton momentum was determined from the deflection of its trajectory by the magnetic field of the machine quadrupoles. Defining the variable $x = p/p_o$, where p is the measured antiproton momentum and p_o the beam momentum, the mass M of the system X is given by $M^2 = (1 - x)s$.

Data were collected with the Collider running in the low-β mode. The acceptance of the forward spectrometer covered the ranges $x \geq .9$ and $.5 \leq -t \leq 1.5$ GeV^2. A momentum resolution of 0.6% (r.m.s. value), was determined from magnetic analysis of elastically scattered particle.

Inelastic diffractive processes can take place if the coherence condition is satisfied, i.e. if the longitudinal momentum transfer is smaller than the inverse of the strong interaction radius. As the centre-of-mass energy increases, this condition becomes satisfied for larger and larger masses. The validity of such classical argument at the energy of the Collider, with production of heavy diffractive states, was shown by the data reported earlier[14], where the typical quasi-elastic peak for $M^2/s \leq .04$ was clearly visible in the invariant differential cross section. At fixed t and for $0.01 \leq M^2/s \leq 0.04$, the $1/M^2$ dependence of the mass distribution already seen in the FNAL and ISR energy range was shown to persist for diffractive states of masses up to more than 100 GeV.

Further information on the features of diffraction dissociation events can be obtained from the study of the produced particles[15]. Pseudo-rapidity distributions of charged tracks from the fragmentation of diffractive states are shown in fig. 3 for several values of the diffractive mass M. An average mass value $\langle M \rangle$ was assigned to each mass interval taking into account the observed $1/M^2$ behaviour and the effect of the mass resolution. Clusters are centered at the expected value $\eta_x = \log(\sqrt{s}/M)$ and their width increases with M in good agreement with the prediction of longitudinal phase space (multiperipheral-type) models and clearly disfavouring isotropic decay (fire-ball) models of the diffractively produced states.

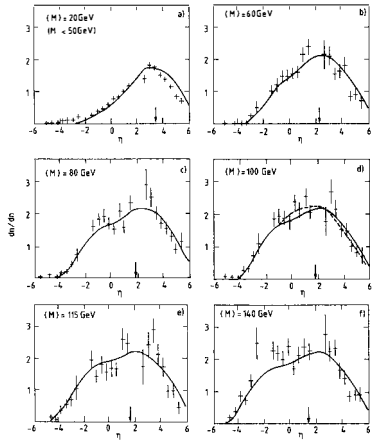

Fig.3 Pseudo-rapidity distribution of charged tracks from the fragmentation of diffractive states. Data are binned in mass intervals with average value ⟨M⟩. The arrows show the position of the centre-of-mass of the diffractive system. The full curves represent the prediction of the DPM (the dashed curve in fig. 3(d) shows the corresponding rapidity distribution).

The similarity of the dissociation of a diffractively produced system of mass M to the hadronization resulting from collisions at c.m.s. energy $\sqrt{s} = M$, is further illustrated in fig. 4. Integration of the pseudorapidity distributions of fig. 3 yields the average multiplicity $\langle n_{ch} \rangle$ of charged secondaries produced in the fragmentation of the X-system. Data from the present experiment are plotted in fig. 4 at $\sqrt{s} = M$ together with a compilation[16] of $\langle n_{ch} \rangle$ as a function of $\sqrt{s}$ for inelastic, non-diffractive, collisions. The growth of $\langle n_{ch} \rangle$ with M closely follows the observed rise of the charged multiplicity with $\sqrt{s}$. However, a closer inspection of fig. 3 shows that, contrary to the case of inelastic pp collisions, the pseudorapidity distribution are not symmetric with respect to the center of mass of the cluster: the average multiplicity in the backward hemisphere (i.e. towards the non-excited $\bar{p}$) is bigger than in the forward one. This asymmetry is similar the one observed in the inelastic πp collisions.

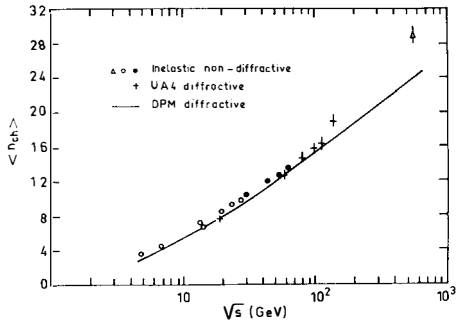

Fig. 4 Average charged multiplicity. The UA4 results for diffractive clusters are plotted at $\sqrt{s} = M$ together with data for inelastic, non-diffractive, events[16]. The curve is the prediction of the DPM discussed in the text.

We shall see in next section as all these features are quantitatively reproduced in the Dual Parton Model (DPM).

2.1 Diffraction dissociation in the Dual Parton Model[17]

In the DPM, high mass single diffractive dissociation is described by the two-chain diagram shown in fig. 5[18]. These two chains or strings are stretched between valence constituents of the excited proton and sea constituents of the non-excited antiproton (which have to form a color singlet). Due to the X^{-1} behaviour of the sea quarks and gluons structure functions, the antiproton inclusive spectrum will have the characteristic $1/(1 - x_p)$ behaviour, typical of a triple-Pomeron Regge approach, well verified by the data as described above. Moreover, at fixed $X = 1 - x_p = M^2/s$ the two chains in the diagram of fig. 5 are identical to those appearing in the dominant (two-chain) component of inelastic $\pi^o p$ scattering at center-of-mass energy $\sqrt{s} = M$ shown in fig. 6. In fact the two chains $q_s - (qq)^p$ and $q_s - q_v^p$ appearing in fig. 5 are the same as those in fig. 6 except that the upper quark and antiquark are from the antiproton-sea. Therefore the momentum distribution functions are in general different in the two cases. However, it turns out that when fixing X, i.e. when fixing the mass M of the diffractive final state, the two momentum distribution functions became identical. In fact in the DPM the joint momentum distribution of a sea quark-antiquark pair is obtained from soft physics arguments (dual Regge behaviour). It was shown[19] that when the x-values of the two members of the pair are equal ($x_1 = x_2$ in fig. 5) one obtains the characteristic x_1^{-1} (for $x_1 \to 0$) behaviour for each of them (the same as in deep-inelastic structure functions). However, when $x_1 \gg x_2$ one obtains a $x_1^{-3/2}$ ($x_2^{-1/2}$) behaviour for the fastest (slowest) member of the sea pair. A momentum distribution function of the sea pair, consistent with the above results can be obtained as follows:

$$\rho(x_1, x_2) = C \int dX\, X^{-1} \int dx\, \rho_q^{\pi}(x)\delta(xX - x_1)\delta((1 - x)X - x_2)$$

$$= \frac{C'}{x_1 + x_2} \frac{1}{(x_1 x_2)^{1/2}}$$

where $\rho_q^{\pi} = x^{-1/2}(1 - x)^{-1/2}$ is the momentum distribution functions of a valence quark in a π[20]. The factor $X^{-1} = (x_1 + x_2)^{-1}$ is typical of sea constituents (both in deep-inelastic structure function and in dual models[21]) and, as mentioned above, gives rise to the standard $(1 - x_p)^{-1}$ form of the diffractive peak. The second term is just the quark momentum distribution functions in a π. It is now obvious that, at fixed $x_1 + x_2 = X$ (i.e. at fixed M), the momentum distribution function of the sea quark-antiquark pair is the same as the one of the valence quark-antiquark pair in a pion with $x_1 + x_2 = X$ instead of $x_1 + x_2 = 1$. Thus, at fixed M, the two chains of the graph in fig. 5 are identical to the corresponding chains in a $\pi^o p$ collision (fig. 6) at center-of-mass energy $\sqrt{s} = M$.

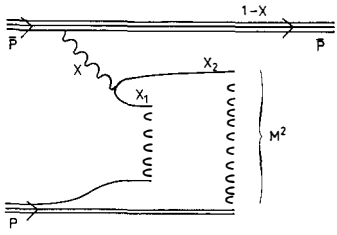

Fig. 5 DPM diagram for high mass diffractive dissociation in $\bar{p}p \to \bar{p}X$ collisions. The wavy line represent a colour singlet (Pomeron) made up of sea partons of the incoming hadron.

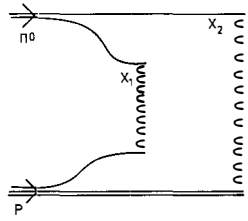

Fig. 6 Two-chain diagram for πp non-diffractive inelastic collisions.

The computation of the rapidity distribution, $dN/dy(M^2)$, of the diffractively produced state of mass M can therefore be performed using the standard convolution[19,20] between momentum distribution functions and fragmentation functions[21] for each of the two chains of fig. 5, and adding them together. The results are compared with the experimental data in fig. 3 where the rapidity has been converted into pseudorapidity using the approach in ref.[22]. In order to reproduce the data in the first mass interval ($M < 50$ GeV), one has to integrate $dN/dy(M^2)$, weighted by $1/M^2$, with the experimental gaussian resolution folded in. This has a negligeable effect in the other mass intervals where one can take a fixed value of M equal to the $\langle M \rangle$ of the considered interval.

The full line in fig. 4 shows the integrated multiplicity computed up to M = 600 GeV using the 2-chain graph of fig. 5 only. As in non-diffractive inelastic collisions, high order contributions containing more chains will become increasingly important with increasing M. The weights of these higher order contributions are not well known. For instance, the ratio of the 4-chain to the 2-chain components is proportional to the ratio of the 4-Pomeron over the 3-Pomeron coupling. If the Pomeron-Pomeron total cross-section is as small as recently estimated[23], we expect that the weights of the multi-chain components will be smaller than for inelastic collisions; multiplicity in diffractive events at M = 546 GeV will then be lower than for non-diffractive events at $\sqrt{s} = M$ (fig. 4).

3. CONCLUSIONS

Data on large-t elastic scattering measured by the UA4 Collaboration at the CERN Collider were reported. The t-ranges covered were $.45 \lesssim -t \lesssim 1.55$ at $\sqrt{s} = 546$ GeV and $.7 \lesssim -t \lesssim 2.2$ at $\sqrt{s} = 630$ GeV. Main feature of these data is the presence of a break in the

$d\sigma/dt$ at $-t \sim .9$ GeV^2 followed by a shoulder with cross section as large as more than one order of magnitude than at the ISR. A comparison of the experimental data with theoretical expectation was done. High energy (ISR and Collider) large-t data were found compatible either with models predicting a non-vanishing odd contribution to the elastic scattering amplitude or with models based on a geometrical picture of the hadron collisions. The geometrical models, however, cannot account for the observed difference between pp and $\bar{p}p$ cross-sections in the dip region as observed at $\sqrt{s} = 53$ GeV. A conclusive statement on the presence of an asymptotically non-vanishing odd term in the hadron elastic scattering amplitude cannot be made before further comparisons between high energy pp and $p\bar{p}$ cross-sections.

A study of diffractive dissociation at the Collider was also presented. Data on pseudorapidity distribution of charged particles produced in the fragmentation of the diffractive states definitively disfavour an isotropic decay (fire-ball like) of these states. It was shown how the Dual Parton Model quantitatively describes multihadron production also in high-mass diffraction dissociation. A prediction was made on the possibility that at higher masses the shown similarity between diffraction dissociation and πp inelastic interaction at $\sqrt{s} = M$ can be broken due to the smaller contribution of higher order multi-chain graphs in diffractive collisions than in non-diffractive inelastic ones.

REFERENCES

1) UA4 Collaboration: D. Bernard, M. Bozzo, P.L. Braccini, F. Carbonara, R. Castaldi, F. Cervelli, G. Chiefari, E. Drago, M. Haguenauer, V. Innocente, P. Kluit, B. Koene, S. Lanzano, G. Matthiae, L. Merola, M. Napolitano, V. Palladino, G. Sanguinetti, P. Scampoli, S. Scapellato, G. Sciacca, G. Sette, R. van Swol, J. Timmermans, C. Vannini, J. Velasco, P.G. Verdini, F. Visco.

2) R. Battiston et al., Nucl. Inst. and Meth. A238 (1985) 38.

3) M. Bozzo et al., Phys. Lett. 147B (1984) 385.

4) M. Bozzo et al., Phys. Lett. 147B (1984) 392.

5) M. Bozzo et al., Phys. Lett. 155B (1985) 197.

6) D. Bernard et al., Phys. Lett. 171B (1986) 142.

7) U. Amaldi et al., Phys. Lett. 66B (1977) 390;
L. Baksay et al., Nucl. Phys. B141 (1978) 1;
G. Barbiellini et al., Phys. Lett. 39B (1972) 663;
A. Bohm et al., Phys. Lett. 49B (1974) 491;
E. Nagy et al., Nucl. Phys. B150 (1979) 221.

REFERENCES (Cont'd)

8) A. Breakstone et al., Nucl. Phys. B248 (1984) 253.

9) S. Erhan et al., Phys. Lett. 152B (1985) 131;
A. Breakstone et al., Phys. Rev. Lett. 54 (1985) 2180.

10) B. Nicolescu, Proc. of the Int. Europhysics Conf. on High Energy Phys., 28-24 July 1985, Bari, Italy.

11) A. Donnachie and P.V.Landshoff, Nucl. Phys B267 (1986) 690.

12) P. Gauron, E. Leader and B. Nicolescu, Phys. Rev. Lett. 54 (1985) 2656, 55 (1985) 639.

13) C. Bourrely,J. Soffer and T.T. Wu, Nucl. Lett. B247 (1984) 15, Phys. Rev. Lett. 54 (1985) 757.

14) M. Bozzo et al., Phys. Lett. 136B (1984) 217.

15) D. Bernard et al., Phys. Lett. 166B (1985) 459.

16) A. Breakstone et al., Phys. Rev. D30 (1984) 528.

17) V. Innocente, A. Capella, A.V. Ramallo and J. Tran Thanh Van, Phys. Lett. 169B (1986) 285.

18) B.R. Desai and U. Sukhatme, A parton approach to peaks at large x in diffractive inclusive reactions, Riverside Univ. preprint;
A. Capella, A. Staar and J. Tran Thanh Van, Phys. Rev. D32 (1985) 2933.

19) A. Capella and J. Tran Thanh Van, Z. Physik 10C (1981) 249.

20) A. Capella, U. Sukhatme, Chung-I Tan and J.Tran Thanh Van, Phys. Lett. 81B (1978) 68;
A. Capella, U. Sukhatme and J. Tran Thanh Van, Z. Physik 3C (1980) 329.

21) A. Capella and J. Tran Thanh Van, Phys. Rev. D29 (1984) 2512.
and references therein.

22) P. Carruthers and Minh Duong-Van, Phys. Rev. D8 (1973) 859.

23) K.H. Streng, Phys. Lett. 166B (1986) 443.